Chemometrics and Intelligent Laboratory Systems 158 (2016) 200–209

Contents lists available at ScienceDirect

Chemometrics and Intelligent Laboratory Systems

journal homepage: www.elsevier.com/locate/chemolab

Multi-way figures of merit in the presence of heteroscedastic and correlated instrumental noise: Unfolded partial least-squares with residual multi-linearization ☆

Franco Allegrini, Alejandro C. Olivieri *

Departamento de Química Analítica, Facultad de Ciencias Bioquímicas y Farmacéuticas, Universidad Nacional de Rosario, Instituto de Química de Rosario (IQUIR-CONICET), Suipacha 531, Rosario S2002LRK, Argentina

ARTICLE INFO

Article history:
Received 7 March 2016
Received in revised form
19 July 2016
Accepted 5 September 2016
Available online 6 September 2016

Keywords:
Unfolded partial least-squares
Residual multi-linearization
Figures of merit
Heteroscedastic noise
Correlated noise

ABSTRACT

In the presence of correlated and/or heteroscedastic noise, i.e., for measurement noise which is not independent and identically distributed (iid), new expressions are required to estimate multi-way calibration figures of merit. They are derived in the present report, with focus towards a useful multi-way approach based on unfolded partial least-squares with residual multi-linearization. The expressions allow one to estimate figures of merit under a generalized noise propagation scenario, and to gain insight into the various uncertainty sources contributing to the overall prediction error and limit of detection. Through the study of both simulated and experimental data, it is shown that significant differences exist between the values estimated assuming an iid noise structure and when the underlying structure deviates from this classical paradigm.

1. Introduction

Multi-way calibration is becoming increasingly popular in the chemical analysis of complex samples, particularly for its ability to cope with uncalibrated interferents [1–3]. This leads to considerably simpler calibration strategies, thanks to the achievement of the second-order advantage, which is potentially inherent to data arrays with at least two different instrumental modes [1]. In the framework of multi-way calibration, research on analytical figures of merit (AFOMs) has made considerable progress in recent years, although the usual assumption has been to consider instrumental errors as independently and identically distributed (iid) [4–8].

Multiple causes may lead to instrumental noise structures which deviate from the simple iid condition [9]. Multi-way AFOM expressions which are valid under this general scenario are required, for a variety of reasons: (1) method development and optimization, (2) comparison of different methodologies, (3) uncertainty reporting along with prediction results, and (4) assessment of detection capabilities. Recently, equations were developed for the prediction uncertainty of first-order multivariate calibration in the presence of generalized noise structures [10], extending previous developments in the field [11].

In the context of multi-way calibration, an approximation has been proposed based on the mean square calibration error which can be achieved by processing second-order data [12]. This latter approach assumes that the measurement noise structure is the same both in calibration and prediction. Moreover, it only considers the overall effect of the noise, with no insight into each of the individual error sources. The present report intends to fill the gap between first-order and multi-way calibration AFOMs for generalized noise structures.

We should first consider the sensitivity, a relevant figure of merit affecting all calibration scenarios [13–15]. Recently, a general sensitivity expression has been discussed, which is able to cover from univariate to multi-way data processing [4]. The strategy to derive the general equation involved the study of the propagation of noise from a test sample to the prediction of the analyte concentration. A very small amount of iid noise was added to a test sample signal, to probe the relative magnitude of the propagation, regardless of the experimental noise structure [4]. Thus, it is reasonable to assume that the sensitivity definition will not change, even when the true noise structure is not iid.

On the other hand, other relevant figures of merit such as prediction uncertainty and detection capabilities may be significantly affected by the noise structure. These parameters should always be reported when developing new analytical protocols [11,16,17]. It might be argued that replicate sample analysis could in principle provide an experimental estimation of these figures. However, it is important to be able to dissect the overall

☆ Selected papers from ThRee-way methods In Chemistry and Psychology conference, 7th edition, 2015.

* Corresponding author.
E-mail address: olivieri@iquir-conicet.gov.ar (A.C. Olivieri).

http://dx.doi.org/10.1016/j.chemolab.2016.09.001
0169-7439/

uncertainty into the different contributing error sources. This could allow one to identify the influence of specific errors, to limit and/or mitigate them, leading to improved analytical results.

In this work, a general scheme is presented to estimate sample dependent uncertainties in a multi-way calibration model based on unfolded partial least-squares with residual multi-linearization (U-PLS/RML). The latter has been widely employed in recent years to process multi-way data achieving the important second-order advantage [18]. To illustrate the usefulness of the proposed expressions, we describe different situations which depend on the structure of the measurement noise. The adequacy of the results was demonstrated through extensive noise addition simulations, and also by application to experimental data sets.

It is hoped that the present report will stimulate further research concerning the estimation of multi-way analytical figures of merit for generalized noise structures when other data processing algorithms are applied, such as multi-linear decomposition [19] or multivariate curve resolution [20].

2. Theory

2.1. U-PLS/RML

The theory of U-PLS/RML is well-known [18]. In the case of three-way/second-order calibration, data matrices are measured for each experimental sample. The (unfolded) test sample signal $\mathbf{x}$ is modeled as the sum of two contributions: (1) the portion of the test signal modeled by the calibration, and (2) the signal from the interferents modeled by RML:

$$\mathbf{x} = \text{Calibration model of } \mathbf{x} + \text{RML model of } \mathbf{x} + e = \\ = \mathbf{P}\mathbf{t}^{\mathrm{T}} + \sum_{n=1}^{N\,\mathrm{int}} \mathbf{c}_{\mathrm{int},n} \otimes \mathbf{b}_{\mathrm{int},n} + \mathbf{e} \tag{1}$$

where $\mathbf{P}$ is the matrix of U-PLS calibration loadings, $\mathbf{t}$ is the test sample scores, the vectors $\mathbf{b}_{\mathrm{int},n}$ and $\mathbf{c}_{\mathrm{int},n}$ are the profiles in each data mode for the nth interferent, N_{int} is the number of interferents, $\otimes$ indicates the Kronecker product, and $\mathbf{e}$ is a vector of model errors (see Table 1 for details on vector and matrix sizes). In Eq. (1), the product $\mathbf{P}\ \mathbf{t}^{\mathrm{T}}$ represents the part of $\mathbf{x}$ which can be modeled by the calibration parameters, while the summation of Kronecker products represents the contribution from the interferents.

Table 1
Parameter symbols, size and details regarding the variables discussed in the present report.

Parameter	Size	Details
$\boldsymbol{\beta}_{\mathrm{eff}}$	$JK \times 1$	Effective U-PLS regression coefficients
$\mathbf{b}_{\mathrm{int},n}$	$J \times 1$	Profile for interferent in the first mode
$\mathbf{c}_{\mathrm{int},n}$	$K \times 1$	Profile for interferent in the second mode
$\mathbf{e}$	$JK \times 1$	Vector of second order RML residuals
$\mathbf{h}$	$1 \times I$	Sample leverage vector
$\mathbf{I}_J$	$J \times J$	Identity matrix
$\mathbf{I}_K$	$K \times K$	Identity matrix
$\mathbf{I}_{JK}$	$JK \times JK$	Identity matrix
$\mathbf{P}$	$JK \times A$	U-PLS loading matrix
$\mathbf{P}_{\mathrm{eff}}$	$JK \times A$	Effective U-PLS loading matrix
$\mathbf{P}_{\mathrm{Zint}}$	$JK \times JK$	Orthogonal projection matrix to $\mathbf{Z}_{\mathrm{int}}$
$\mathbf{t}$	$1 \times A$	Sample score vector
$\mathbf{T}$	$I \times A$	Calibration score matrix
$\mathbf{X}$	$I \times JK$	Calibration data matrix
$\mathbf{x}$	$JK \times 1$	Test data vector (after unfolding the data matrix)
$\mathbf{v}$	$A \times 1$	Vector of latent U-PLS regression coefficients
$\mathbf{y}_{\mathrm{cal}}$	$I \times 1$	Calibration concentrations
$\mathbf{Z}_{\mathrm{int}}$	$JK \times N_{\mathrm{int}}(J+K)$	Matrix spanning the interferent space
$\boldsymbol{\Sigma}^2_{\mathrm{x}}$	$JK \times JK$	Error covariance matrix for test sample
$\boldsymbol{\Sigma}^2_{\mathrm{X}}$	$JK \times JK$	Error covariance matrix for calibration samples
$\boldsymbol{\Sigma}^2_{\mathrm{X},i}$	$JK \times JK$	Error covariance matrix for calibration sample i
$\boldsymbol{\Sigma}^2_{\mathrm{X,eff}}$	$JK \times JK$	Effective error covariance matrix for calibration

The aim of the RML procedure is to find the score vector $\mathbf{t}$ minimizing the norm of the vector $\mathbf{e}$ in Eq. (1), rendering at the same time the interferent profiles in each data mode. Once $\mathbf{t}$ is found by RML, prediction of the analyte concentration $\hat{y}$ proceeds through:

$$\hat{y} = \mathbf{t}\,\mathbf{v} = \mathbf{t}\ \mathbf{T}^{+}\mathbf{y}_{\mathrm{cal}} \tag{2}$$

where $\mathbf{v}$ is the vector of latent regression coefficients provided by the U-PLS calibration model, $\mathbf{T}$ is the matrix of calibration scores, $\mathbf{y}_{\mathrm{cal}}$ the vector of analyte calibration concentrations and '+' indicates the pseudo-inverse operation. An analogous expression to Eq. (1) holds for higher-order data [18].

2.2. Prediction uncertainty

A general expression for prediction uncertainty using U-PLS/RML is derived in this section. It can be easily extended for further multi-way data systems. In the most general scenario, noise affects both calibration and test sample signals and calibration concentrations, and hence differentiation of Eq. (1) leads to:

$$d\mathbf{x} = d\mathbf{P}\ \mathbf{t}^{\mathrm{T}} + \mathbf{P}\ d\mathbf{t}^{\mathrm{T}} + d\left(\sum_{n=1}^{N\,\mathrm{int}} \mathbf{c}_{\mathrm{int},n} \otimes \mathbf{b}_{\mathrm{int},n}\right) \tag{3}$$

The last term of Eq. (3) can be shown to be the product of a matrix $\mathbf{Z}_{\mathrm{int}}$ representing the space spanned by the interferents and a column vector containing the differentials $d\mathbf{c}_{\mathrm{int},n}$ and $d\mathbf{b}_{\mathrm{int},n}$ (see Appendix), i.e.:

$$d\mathbf{x} = d\mathbf{P}\ \mathbf{t}^{T} + \mathbf{P}d\mathbf{t}^{T} + \mathbf{Z}_{\mathrm{int}}\left[d\mathbf{b}_{\mathrm{int},1};\ d\mathbf{c}_{\mathrm{int},1};\ d\mathbf{b}_{\mathrm{int},2};\ d\mathbf{c}_{\mathrm{int},2};\ \ldots\right] \tag{4}$$

where the usual MATLAB notation ';' is employed to append column vectors on top of each other [21], and $\mathbf{Z}_{\mathrm{int}}$ is given by:

$$\mathbf{Z}_{int} = [\mathbf{c}_{\mathrm{int},1} \otimes \mathbf{I}_J,\ \otimes\ \mathbf{I}_K \otimes \mathbf{b}_{\mathrm{int},1},\ \mathbf{c}_{\mathrm{int},2} \otimes \mathbf{I}_J,\ \mathbf{I}_K \otimes \mathbf{b}_{\mathrm{int},2},\ \ldots] \tag{5}$$

where the ',' appends matrices adjacent to each other, and $\mathbf{I}_J$ and $\mathbf{I}_K$ are $J \times J$ and $K \times K$ identity matrices respectively. This suggest that the last term in Eq. (4) can be removed by multiplication by a suitable projection matrix, orthogonal to $\mathbf{Z}_{\mathrm{int}}$:

$$\mathbf{P}_{Z\mathrm{int}}d\mathbf{x} = \mathbf{P}_{Z\mathrm{int}}d\mathbf{P}\ \mathbf{t}^{T} + \mathbf{P}_{Z\mathrm{int}}\mathbf{P}d\mathbf{t}^{T} \tag{6}$$

where $\mathbf{P}_{Z\mathrm{int}} = (\mathbf{I}_{JK} - \mathbf{Z}_{\mathrm{int}}\ \mathbf{Z}_{\mathrm{int}}{}^{+})$ and $\mathbf{I}_{JK}$ is an identity matrix of size $JK \times JK$. From Eq. (6):

$$d\mathbf{t} = [d\mathbf{x}^{T} - \mathbf{t}d\mathbf{P}^{T}]\mathbf{P}_{Z\mathrm{int}}\left(\mathbf{P}_{Z\mathrm{int}}\mathbf{P}\right)^{+T} \tag{7}$$

Since $\mathbf{P}^{\mathrm{T}} = \mathbf{T}^{+}\ \mathbf{X}$, where $\mathbf{X}$ is the matrix of calibration (unfolded) signals, differentiation of $\mathbf{P}$ and replacement in Eq. (7) gives:

$$d\mathbf{t} = \left\{ d\mathbf{x}^{T} - \mathbf{t}\left[\mathbf{T}^{+}d\mathbf{X} + d\left(\mathbf{T}^{+}\right)\mathbf{X}\right]\right\}\mathbf{P}_{Z\mathrm{int}}\left(\mathbf{P}_{Z\mathrm{int}}\mathbf{P}\right)^{+T} \tag{8}$$

We now focus attention on the expression for the differential change in predicted concentration, starting from Eq. (2):

$$d\hat{y} = d(\mathbf{t}\mathbf{T}^{+}\mathbf{y}_{\mathrm{cal}}) = \mathbf{t}d(\mathbf{T}^{+})\mathbf{y}_{\mathrm{cal}} + (d\mathbf{t})\mathbf{T}^{+}\mathbf{y}_{\mathrm{cal}} + \mathbf{t}\mathbf{T}^{+}d\mathbf{y}_{\mathrm{cal}} \tag{9}$$

And inserting in the latter equation $d\mathbf{t}$ from Eq. (8):

$$\begin{aligned} d\hat{y} = {} & \mathbf{t}d(\mathbf{T}^{+})\mathbf{y}_{\mathrm{cal}} + (d\mathbf{x}^{\mathrm{T}})\mathbf{P}_{Z\mathrm{int}}(\mathbf{P}_{Z\mathrm{int}}\mathbf{P})^{+\mathrm{T}}\mathbf{T}^{+}\mathbf{y}_{\mathrm{cal}} \\ & - \mathbf{t}\mathbf{T}^{+}d\mathbf{X}\mathbf{P}_{Z\mathrm{int}}(\mathbf{P}_{Z\mathrm{int}}\mathbf{P})^{+\mathrm{T}}\mathbf{T}^{+}\mathbf{y}_{\mathrm{cal}} - \\ & - \mathbf{t}d(\mathbf{T}^{+})\mathbf{X}\mathbf{P}_{Z\mathrm{int}}(\mathbf{P}_{Z\mathrm{int}}\mathbf{P})^{+\mathrm{T}}\mathbf{T}^{+}\mathbf{y}_{\mathrm{cal}} + \mathbf{t}\mathbf{T}^{+}d\mathbf{y}_{\mathrm{cal}} \end{aligned} \tag{10}$$

In the latter equation, two important changes can be made: (1) the factor $\mathbf{P}_{Z\mathrm{int}}\ (\mathbf{P}_{Z\mathrm{int}}\ \mathbf{P})^{+\mathrm{T}}$ can be condensed as $\mathbf{P}_{\mathrm{eff}}{}^{+\mathrm{T}}$, where

$\mathbf{P}_{\text{eff}}$ is an effective loading matrix given by $\mathbf{P}_{\text{eff}}=\mathbf{P}_{\text{Zint}}\ \mathbf{P}$ [22], and (2) the product $\mathbf{P}_{\text{Zint}}\ \mathbf{P}_{\text{eff}}{}^{+\text{T}}\ \mathbf{T}^{+}\mathbf{y}_{\text{cal}}=\mathbf{P}_{\text{eff}}{}^{+\text{T}}\ \mathbf{T}^{+}\mathbf{y}_{\text{cal}}$ is an effective vector of regression coefficients $\boldsymbol{\beta}_{\text{eff}}$, valid in the presence of interferents [22]. Therefore, the first term of the right hand side of Eq. (10) is approximately equal to the fourth one, because the latter is equal to $-\mathbf{t}d(\mathbf{T}^{+})\mathbf{X}\ \boldsymbol{\beta}_{\text{eff}}=-\mathbf{t}d(\mathbf{T}^{+})\,\hat{\mathbf{y}}_{\text{cal}}$ ($\hat{\mathbf{y}}_{\text{cal}}$ is the vector of calibration concentrations estimated by the U-PLS model). The approximate equality of the first and fourth terms of Eq. (10) is valid in case the model is unbiased, which is usually expected if the rank of the system is well estimated. If this condition is fulfilled, the mean value of $(\mathbf{y}_{\text{cal}}-\hat{\mathbf{y}}_{\text{cal}})$ will tend to zero, leading to the cancellation of both terms. In such a case, and introducing the sample leverage vector $\mathbf{h}=\mathbf{t}\ \mathbf{T}^{+}$, Eq. (10) reduces to the sought three-term expression:

$$d\hat{y} = (d\mathbf{x}^{\text{T}})\boldsymbol{\beta}_{\text{eff}} - \mathbf{h}d\mathbf{X}\boldsymbol{\beta}_{\text{eff}} + \mathbf{h}d\mathbf{y}_{\text{cal}} \tag{11}$$

These three terms are not correlated to each other, so they will contribute independently to the prediction variance (the expectation value of the cross-products between $d\mathbf{x}$ and $d\mathbf{X}$ is expected to be negligible, since noise from different samples is uncorrelated). The variance in predicted concentration is thus the following expectation value:

$$E(d\hat{y}^2) = E\left[\boldsymbol{\beta}_{\text{eff}}^{\text{T}}(d\mathbf{x}d\mathbf{x}^{\text{T}})\boldsymbol{\beta}_{\text{eff}} - \boldsymbol{\beta}_{\text{eff}}^{\text{T}}d\mathbf{X}^{\text{T}}\mathbf{h}^{\text{T}}\mathbf{h}d\mathbf{X}\boldsymbol{\beta}_{\text{eff}} + \mathbf{h}d\mathbf{y}_{\text{cal}}d\mathbf{y}_{\text{cal}}^{\text{T}}\mathbf{h}^{\text{T}}\right] \tag{12}$$

The first term of Eq. (12) adopts a particularly simple form, since the expected value of the product $(d\mathbf{x}\ d\mathbf{x}^{\text{T}})$ is the error covariance matrix for the test sample signals $\boldsymbol{\Sigma}_{\text{x}}^{2}$. In the second term, on the other hand, the expectation value of the product $(d\mathbf{X}^{\text{T}}\ \mathbf{h}^{\text{T}}\ \mathbf{h}\ d\mathbf{X})$ can be shown to lead to an effective covariance matrix $(\boldsymbol{\Sigma}_{\text{X,eff}}^{2})$ for the calibration signals. Details about the derivation to arrive to the effective covariance matrix can be found in the Supporting Information of ref. [10]. However, the important concept to be remarked in this context is that the effective covariance matrix $\boldsymbol{\Sigma}_{\text{X,eff}}^{2}$ is a weighted average of all error covariance matrices for the calibration set of samples.

The last term in Eq. (12) is the variance in calibration concentrations σ_{ycal}^{2}. Thus, the above study confirms that the prediction variance is given by the three-term expression:

$$\sigma_{\hat{y}}^{2} = \boldsymbol{\beta}_{\text{eff}}^{\text{T}}\boldsymbol{\Sigma}_{\text{x}}^{2}\boldsymbol{\beta}_{\text{eff}} + h\boldsymbol{\beta}_{\text{eff}}^{\text{T}}\boldsymbol{\Sigma}_{\text{X,eff}}^{2}\boldsymbol{\beta}_{\text{eff}} + h\sigma_{\text{ycal}}^{2} \tag{13}$$

which accounts for all types of noise structures, and covers the case where the error structure varies from sample to sample. In the event of non-iid noise, but with all error covariance matrices (calibration and prediction samples) identical, Eq. (13) simplifies to:

$$\sigma_{\hat{y}}^{2} = \boldsymbol{\beta}_{\text{eff}}^{\text{T}}\boldsymbol{\Sigma}_{\text{x}}^{2}\boldsymbol{\beta}_{\text{eff}} + h\boldsymbol{\beta}_{\text{eff}}^{\text{T}}\boldsymbol{\Sigma}_{\text{x}}^{2}\boldsymbol{\beta}_{\text{eff}} + h\sigma_{\text{ycal}}^{2} \tag{14}$$

Finally, when the error structure is iid, $\boldsymbol{\Sigma}_{\text{X,eff}}^{2}$ collapses to $\boldsymbol{\Sigma}_{\text{X}}{}^{2}\mathbf{I}_{M}$ and Eq. (14) gives:

$$\sigma_{\hat{y}}^{2} = \sigma_{\text{x}}^{2}\boldsymbol{\beta}_{\text{eff}}^{\text{T}}\boldsymbol{\beta}_{\text{eff}} + h\sigma_{\text{x}}^{2}\boldsymbol{\beta}_{\text{eff}}^{\text{T}}\boldsymbol{\beta}_{\text{eff}} + h\sigma_{\text{ycal}}^{2} \tag{15}$$

which is formally analogous to that proposed by Faber and Kowalski for first-order PLS calibration [11]. Since the multi-way U-PLS/RML sensitivity SEN can be defined as $1/\|\boldsymbol{\beta}_{\text{eff}}\|$ (where $\|\ \|$ indicates the vector norm) [4], Eq. (15) can also be written in the familiar form:

$$\sigma_{\hat{y}}^{2} = \sigma_{\text{x}}^{2}\text{SEN}^{-2} + h\sigma_{\text{x}}^{2}\text{SEN}^{-2} + h\sigma_{\text{ycal}}^{2} \tag{16}$$

The latter expression has been employed in several analytical works resorting to U-PLS/RML calibration in the past, although the rigorous derivation is only presented here. Two aspects of the present approach deserve attention in the framework of multi-way data processed by U-PLS/RML. On one hand, the position of the sample in the calibration space, in what concerns prediction uncertainty, is measured by a leverage parameter h, computed by first removing the contribution of the interferents, and not from the global test sample data. This is clear in Eq. (12), where the $\mathbf{h}=\mathbf{t}\ \mathbf{T}^{+}$, with $\mathbf{t}$ obtained by the RML procedure during modeling of the interferent signals. On the other hand, the effect of the interferents is present in Eq. (13) through the effective vector of regression coefficients $\boldsymbol{\beta}_{\text{eff}}$. Any interfering signal, overlapping with those from the analytes, will lead to a decrease of the sensitivity of the determination by modifying the value of $\boldsymbol{\beta}_{\text{eff}}$.

In the most general U-PLS/RML scenario, i.e., when residual multi-linearization is employed to model interferents in multi-way data of any number of instrumental modes, the prediction uncertainty equation is identical to Eq. (13).

It is important to remark that the error structure information is being used in the evaluation of prediction uncertainty, but it could be argued that it should also appear in the PLS/RML procedure itself. Minimizing the norm of the residuals assumes an iid structure for optimal results, which is not the case. In first-order calibration, this has been solved with the development of a maximum likelihood version of principal component regression (MLPCR), with a significant improvement in comparison with classical PCR/PLS in different spectroscopic systems [23–25]. This may imply the need of developing a similar multi-way maximum likelihood strategy, but this is outside the scope of the present work. However, the lack of an optimal multi-way PLS model to deal with non-iid noise structures does not imply that satisfactory predictions cannot be obtained in the presence of modest deviations. This justifies one of the main objectives of this work: to show how these modest deviations affect the sample dependent prediction uncertainty.

Another important aspect to be considered is that Eq. (16) could be extended to a potential multi-way maximum likelihood model as the one previously proposed. Support to this observation is given by a recent publication [26] where a general expression to calculate analytical sensitivity under different noise structures was presented, together with a first attempt to extend Eq. (16) to calculate prediction uncertainties when first-order MLPCR is used as a predictive model.

2.3. Practical implications: limits of detection and quantitation

It has been recently shown that the limit of detection in first-order PLS calibration can be reported as a range of values, which depend on the varying composition of the blank [27].

$$\text{LOD}_{\text{min}} = 3.3\ [\text{SEN}^{-2}\ \sigma_{\text{x}}^{2} + h_{0\text{min}}\text{SEN}^{-2}\ \sigma_{\text{x}}^{2} + h_{0\text{min}}\ \sigma_{\text{ycal}}^{2}]^{1/2} \tag{17}$$

$$\text{LOD}_{\text{max}} = 3.3\ [\text{SEN}^{-2}\ \sigma_{\text{x}}^{2} + h_{0\text{max}}\text{SEN}^{-2}\ \sigma_{\text{x}}^{2} + h_{0\text{max}}\ \sigma_{\text{ycal}}^{2}]^{1/2} \tag{18}$$

In the above expressions, $h_{0\text{min}}$ and $h_{0\text{max}}$ are the maximum and minimum, respectively, of the leverages for the calibration samples projected onto the plane of zero analyte concentration [27]:

$$h_{0\,\text{min}} = \frac{\bar{y}_{\text{cal}}^{2}}{\sum_{i=1}^{Ical} y_{i}^{2}} \tag{19}$$

$$h_{0\,\text{max}} = \max\left\{h_{i} + h_{0\,\text{min}}\left[1 - \left(\frac{y_{\text{i}}}{\bar{y}_{\text{cal}}}\right)^{2}\right]\right\} \tag{20}$$

where $\bar{y}_{\text{cal}}$ is the mean calibration concentration, y_i is the centered concentration for the ith calibration sample, I_{cal} is the number of

calibration samples, and h_i is the leverage of a generic calibration sample. For mean-centered data, the effective leverages ($h_{0min}+1/I_{cal}$) and ($h_{0max}+1/I_{cal}$) should be employed in Eqs. (20) and (21).

Analogous expressions are valid for the limit of quantitation [27]:

$$LOQ_{min} = 10\,[SEN^{-2}\,\sigma_x^2 + h_{0min}SEN^{-2}\,\sigma_x^2 + h_{0min}\,\sigma_{ycal}^2]^{1/2} \quad (21)$$

$$LOQ_{max} = 10\,[SEN^{-2}\,\sigma_x^2 + h_{0max}SEN^{-2}\,\sigma_x^2 + h_{0max}\,\sigma_{ycal}^2]^{1/2} \quad (22)$$

An essential condition for the application of these expressions, is that the composition of the test samples should be well represented by the composition of calibration samples. In principle it could be stated that, because of the presence of unexpected components in test samples, the latter condition will not be fulfilled by most multi-way systems. However, the previous difficulty is automatically solved by the RML procedure by filtering the effect of the unexpected components, and making the unknown sample scores part of the calibration space. In consequence, these definitions could be directly extended to the multi-way version of PLS (U-PLS/RML) without further developments.

Considering the general equation to calculate sample dependent prediction uncertainty derived in Section 2.2, it is possible to extend the previous detection limit definitions to non-iid error structures. The corresponding equations would be as follows:

$$LOD_{min}=3.3\,[\boldsymbol{\beta}_{eff}^2\boldsymbol{\Sigma}_x^2\boldsymbol{\beta}_{eff}^2+h_{0min}\boldsymbol{\beta}_{eff}^2\boldsymbol{\Sigma}_{X,eff}^2\boldsymbol{\beta}_{eff}^2+h_{0min}\sigma_{ycal}^2]^{1/2}. \quad (23)$$

$$LOD_{max}=3.3[\boldsymbol{\beta}_{eff}^2\boldsymbol{\Sigma}_x^2\boldsymbol{\beta}_{eff}^2+h_{0max}\boldsymbol{\beta}_{eff}^2\boldsymbol{\Sigma}_{X,eff}^2\boldsymbol{\beta}_{eff}^2+h_{0max}\sigma_{ycal}^2]^{1/2} \quad (24)$$

2.4. Practical implications: generalized analytical sensitivity

As mentioned in Section 2.2, a recent work proposed a new version of the analytical sensitivity, which incorporates the noise properties in its definition, and is well correlated with average prediction errors. To be consistent with the traditional sensitivity in terms of units, this new definition states that a generalized analytical sensitivity (GAS) can be defined as the inverse of the first term of the general prediction uncertainty equation [analogous of Eq. (16) for first-order calibration] [26]. In this sense, the derivation presented in Section 2.2 provides a formal background for the calculation of GAS in the context of multi-way calibration using the UPLS-RML model.

3. Data sets

3.1. Simulated data

Multi-way synthetic data sets were generated using noiseless Gaussian profiles to simulate the response of the components in each instrumental mode. These profiles were normalized and then used to create the corresponding multi-way arrays. They were then multiplied by the corresponding calibration and test concentrations to obtain calibration and test sample arrays. The concentrations consisted of random numbers in the range of 0–1, with 10 calibration samples and 4 test samples.

Following the same scheme as the one described in ref. [8], the number of analytes (present in both calibration and test samples) and interferents (only present in test samples) were combined to generate different kinds of binary (two components), ternary (three components) and quaternary (four components) systems. Sensitivity was also varied, changing the positions of the peaks in each mode with respect to the position of the peak corresponding to the analyte to be quantified. The dimensions for each simulated instrumental mode were: $J=30$, $K=30$ for second-order systems, $J=20$, $K=20$, $L=20$ for third-order systems, and $J=10$, $K=10$, $L=10$, $M=10$, for fourth-order systems.

The code to generate the simulations was written using MATLAB version 7.4.0 (R2007a) [21], using the Parallelization Toolbox to increase calculation speed. This latter factor turned out to be critical as the data order increases.

3.2. Noise addition

In agreement with the generalized proposal presented in ref. [10] for first-order calibration, two types of typical noise structures were used to evaluate the deviation from iid paradigm: (1) pink noise, to analyze the violation of the condition of independence, and (2) proportional noise, to analyze the divergence from the "identically distributed" condition.

In all cases, noise was simulated by adding a vector corresponding to the type of noise under study to each unfolded matrix. For pink noise, the MATLAB function presented in ref. [10] was used to generate a noise vector of a size matching the dimensions of the unfolded data arrays. This noise sequence was scaled in such a way that its standard deviation ranged between 5% and 10% of the mean spectral intensity calculated for the calibration samples. In the case of proportional noise, the sequence was generated by multiplying each unfolded array both by a scaling factor of 0.01, and by a number randomly extracted from a normal distribution. In other words, the noise at each sensor of the unfolded matrix will be 1% of the signal intensity at that particular sensor.

As the data order increases, the error structure elucidation becomes more complex. This means that, for example, different types of correlations could appear along the different data modes and also between them. As a consequence, some types of noise (as $1/f$ or pink noise), are unlikely to extend over multiple modes in a smooth fashion, as proposed in the present simulations. Indeed, it is more likely that some type of block diagonal structure would be observed for the error covariance matrix. In any case, although the simulations may not exactly represent a particular real case, the simplification could be considered as sufficient to the aim of deriving conclusions based on error propagation.

Noise can be added not only with the purpose of evaluating a particular error structure, but also to investigate the effect of the different error propagation sources contributing to the final uncertainty, i.e.: (1) uncertainty propagated only from errors in test sample signals, (2) uncertainty propagated only from errors in calibration sample signals, (3) uncertainty propagated only from errors in calibration concentrations, and (4) uncertainty propagated from all error sources together. It is important to remark that systems containing iid noise were not studied in this work, because this analysis has been previously reported in the literature in the context of a proposal of a new expression for sensitivity calculation in U-PLS/RML [8].

Overall, for each type of noise, 960 different systems were studied, corresponding to 3 different data orders, 6 systems with varying number of analytes and interferent agents, 4 different component concentrations, and 10 different sensitivities which depended on the degree of spectral overlap.

3.3. Experimental data

The experimental system analyzed in this work corresponds to synchronous fluorescence spectra measured in a flow-injection analysis (FIA) system with double pH gradient modulation. The double pH gradient was generated with a peristaltic pump, which drives an acid carrier through a Teflon tube. After the injection of an alkaline sample, the flow is sent to a spectrofluorometer flow cell. The start of the spectral measurements is determined by the

injection time. Between the possible procedures to generate the pH gradient inside a flow stream, the one selected was to inject the alkaline sample into the acid sample used as the carrier. While the sample was flowing through the measuring cell, synchronous fluorescence spectra were collected under the following conditions: (1) constant difference between excitation and emission monochromators, 175 nm; (2) emission wavelength range, 425–525 nm each 1 nm; excitation wavelength range, 250–350 nm each 1 nm; time between successive spectra, 30 s; total time, 10.5 min.

The measurements previously described lead to a second-order system where a matrix is obtained for each sample. One of the instrumental modes corresponds to fluorescence spectra and the other to different times at which pH is modified following a gradient. This is why the latter data mode could be called as either "pH" or "time". For simplicity, in the remainder of this work, we will refer to this mode as the "time" mode. These second-order data were used for the determination of three analytes in human urine: the antibiotics ciprofloxacin, norfloxacin, and ofloxacin. The calibration was developed using aqueous solutions of each of the three analytes in turn. In this case, the use of U-PLS/RML is justified by the presence of a fluorescent urine background that makes it necessary to achieve the second-order advantage.

For each analyte, the calibration set was prepared with five duplicate concentration levels, equally spaced in the range 0.00–1.00 mg L^{-1}. The urine set consisted on 22 test samples spiked at concentrations given by random numbers in the range 0–200 mg L^{-1}, to test the method performance for many concentrations within the therapeutic range. All samples were measured in random order. For additional experimental details see ref. [28].

4. Results and discussion

4.1. Estimation of the error covariance matrix

Experimental replication consists in taking N replicate measurement vectors $\mathbf{x}_n$ and then calculating the error covariance matrix as:

$$\mathbf{\Sigma}_x^2 = \frac{1}{N-1}\sum_{n=1}^{N}(\mathbf{x}_n - \bar{\mathbf{x}})(\mathbf{x}_n - \bar{\mathbf{x}})^T \tag{25}$$

The error covariance matrix is a symmetric square matrix containing, as diagonal elements, the error variances associated with each measurement channel, and as off-diagonal elements, all of the covariances among measurement errors at different sensors [9]. For the analysis of the error structure, the diagonal of the covariance matrix gives information about the noise heteroscedasticity, whereas the off-diagonal values describe the nature of the correlated noise.

A good approach to estimating $\mathbf{\Sigma}_x^2$ involves pooling the error covariance estimates by averaging the calculated covariance matrix from different subsets of samples, each of which has a relatively small number of replicates [29]. Theoretical prediction of the error covariance matrix is also possible for simulated data and for certain experimental data sets in which the error sources are well characterized. This strategy was employed for the simulated data sets used in this work.

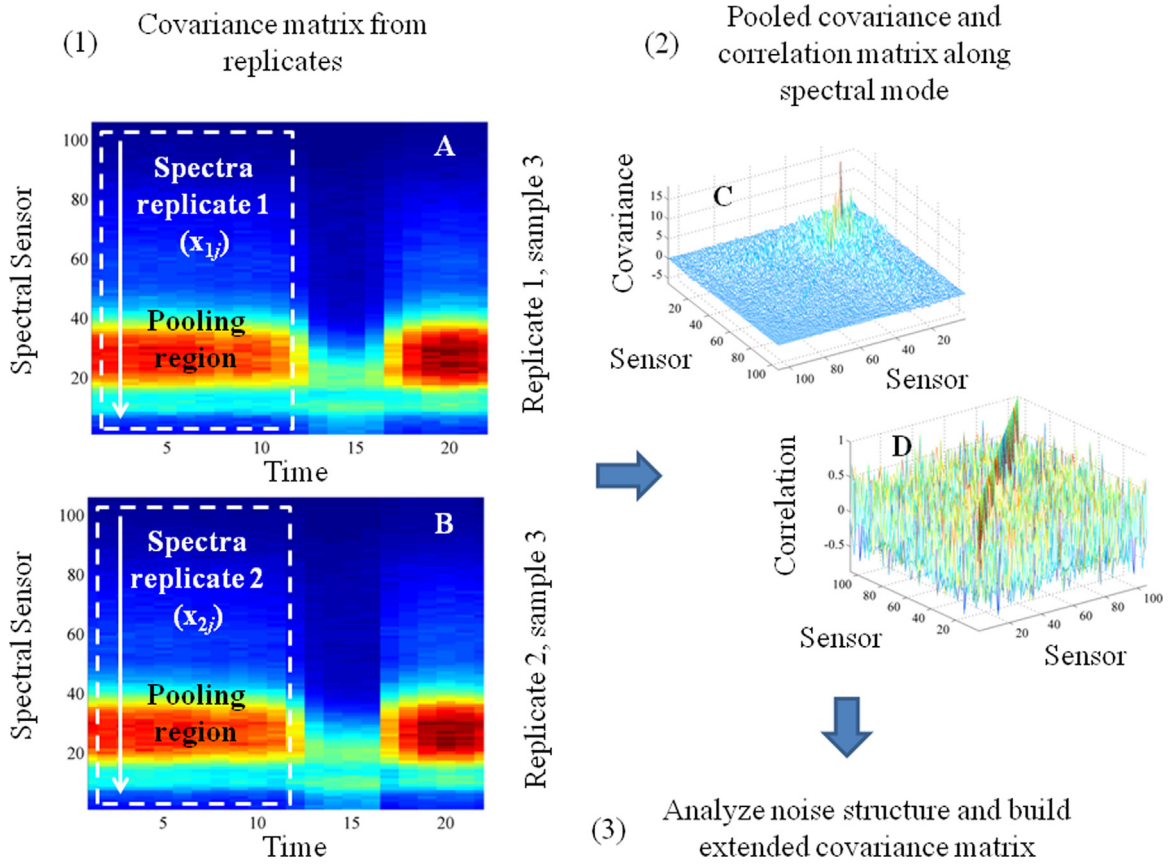

Fig. 1. Steps of the procedure designed to analyze the error structure of experimental second-order data with a minimum number of replicates per sample. (A) and (B) color map of the data matrices corresponding to two replicates of a calibration sample used for ciprofloxacin determination. (C) Resulting pooled error covariance matrix for the same calibration sample, when the spectra corresponding to pH with similar signal variation are considered as a pooling subset. (D) Error correlation matrix.

To analyze the error structure of the experimental data, the error sources were determined using an alternative pooling strategy (Fig. 1). The latter was designed considering two limiting factors: (1) the small number of replicates, and (2) the significant difference in spectral intensity from sample to sample, which limits the possibility of building pools from different subsets of samples. In response to these limitations, a region was selected from a given data matrix of the same pool (pooling region in Fig. 1), where the spectral variation from sample to sample was not significant.

The procedure basically consists in two steps: an error covariance matrix is first built from the spectra extracted for a certain time using both replicates. This step is repeated for each of the spectra belonging to the pooling region, and can be summarized by the following expression:

$$\Sigma^2_j = \sum_{n=1}^{N} (\mathbf{x}_{nj} - \bar{\mathbf{x}}_j)(\mathbf{x}_{nj} - \bar{\mathbf{x}}_j)^T \quad (26)$$

where $\mathbf{\Sigma}^2_j$ is a covariance matrix calculated from the spectral replicates at time j, $\mathbf{x}_{nj}$ is the spectrum for replicate n and time j, and $\bar{\mathbf{x}}_j$ the mean spectrum calculated for both replicates at time j. As these latter matrices are obtained using a minimum number of replicates, they are extremely noisy. To sort out this difficulty, a second step is added, where a covariance matrix is built by pooling the covariance matrices obtained in the previous step. The expression to calculate this matrix is:

$$\mathbf{\Sigma}^2_{pools} = (\mathbf{\Sigma}^2_1 + \mathbf{\Sigma}^2_2 + \ldots \mathbf{\Sigma}^2_j)/J_r \quad (27)$$

where $\mathbf{\Sigma}^2_{pools}$ is the pooled covariance matrix for the sth sample and J_r is the number of time points included in the pooling region (see Fig. 1).

Eq. (27) provides a model of the error structure with considerably smaller noise, and is a valid resource as a first stage to infer about the error structure along the spectral mode of this particular data set. However, it is important to remark that this is not a general strategy to model an error covariance matrix, because it depends on the similarity of spectra at different times, which is a condition that may not be fulfilled in other kinds of higher-order data sets.

The inspection of the error covariance matrix obtained by the methodology previously described (Fig. 1) constitutes a first visual evidence that spectral proportional noise along the spectral mode is the main error source affecting the system. At the same time, the correlation matrix shows that there is a low correlation along the spectral mode.

To rationalize this observation, the mean signal intensity in the pooling region was plotted against the standard deviation of that signal at each spectral sensor. Fig. 2 confirms the previous suspicion, since the observed trend is the expected one for proportional noise: as the intensity increases, the standard deviation of the signal increases. Although the results are only shown for one calibration concentration (200 mg L^{-1}), the trend is the same for the remaining concentration values.

Once the main error source is identified, the final step is to build an extended covariance matrix. As the error structure is mainly heteroscedastic, this matrix will have non-zero elements only along its diagonal. In the event that correlation is present, the error covariance matrix will incorporate non-zero off-diagonal elements. However, this would require a further analysis concerning a possible error structure along the time direction. To perform this analysis in this particular data set in a reliable way, a larger number of replicates would be necessary. The reason is that the number of sensors showing a similar temporal profile is not large enough to apply the described pooling strategy for the remaining data mode. In any case, the results presented in Section 4.4. (Fig. 5), suggest that if an extra correlation exists along the temporal profiles, its contribution to the final prediction error is not significant.

To calculate the scaling factor to adapt the intensity of the signals to the intensity of the noise, a weighted linear regression of the diagonal of $\mathbf{\Sigma}^2_{pools}$ against the spectra of the corresponding sample was performed. The weights were determined as the standard deviation calculated considering the variation of each sensor in the time direction.

4.2. Simulated data

As shown in previous works, a reasonable strategy to validate an expression derived from the uncertainty propagation approach is to contrast its prediction with the uncertainty obtained by iterative noise addition simulations [10]. If the equation yields the expected result, the points representing test samples predicted under different calibrations and variable conditions of noise addition will lie near the ideal equality line.

Figs. 3 and 4 show a comparison between uncertainty estimated by Eq. (17) (first column) and (19) (second column) and the standard deviation obtained by iterative noise addition simulations. This comparison was performed for different data orders using the pertinent algorithm, namely second-order U-PLS/RML (A and B), third-order U-PLS/RML (C and D), and fourth-order U-PLS/RML (E and F). By inspection of the plots in these figures, it is apparent that when the specific error structure affecting the system is included in the equation used to predict the uncertainty through the error covariance matrix [Eq. (17)], the results nearly perfectly match those obtained by noise addition simulations.

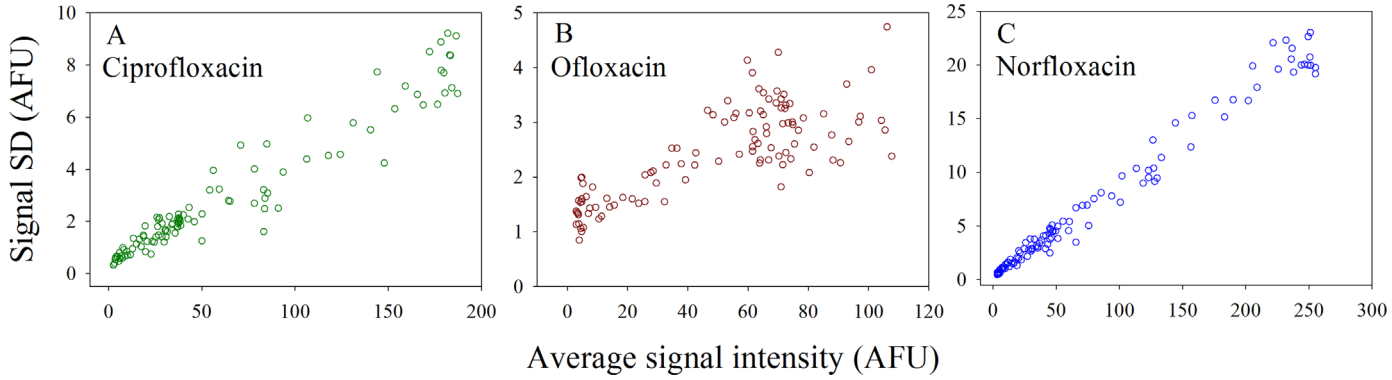

Fig. 2. Signal standard deviation against average signal intensity, calculated for the pooling region (see Fig. 1) using the experimental calibration matrices at a specific concentration for the quantification of each analyte. (A) Ciprofloxacin 200 mg L^{-1}. (B) Ofloxacin 200 mg L^{-1}. (C) Norfloxacin 200 mg L^{-1}. The values are given in arbitrary fluorescence units (AFU). SD: Standard Deviation.

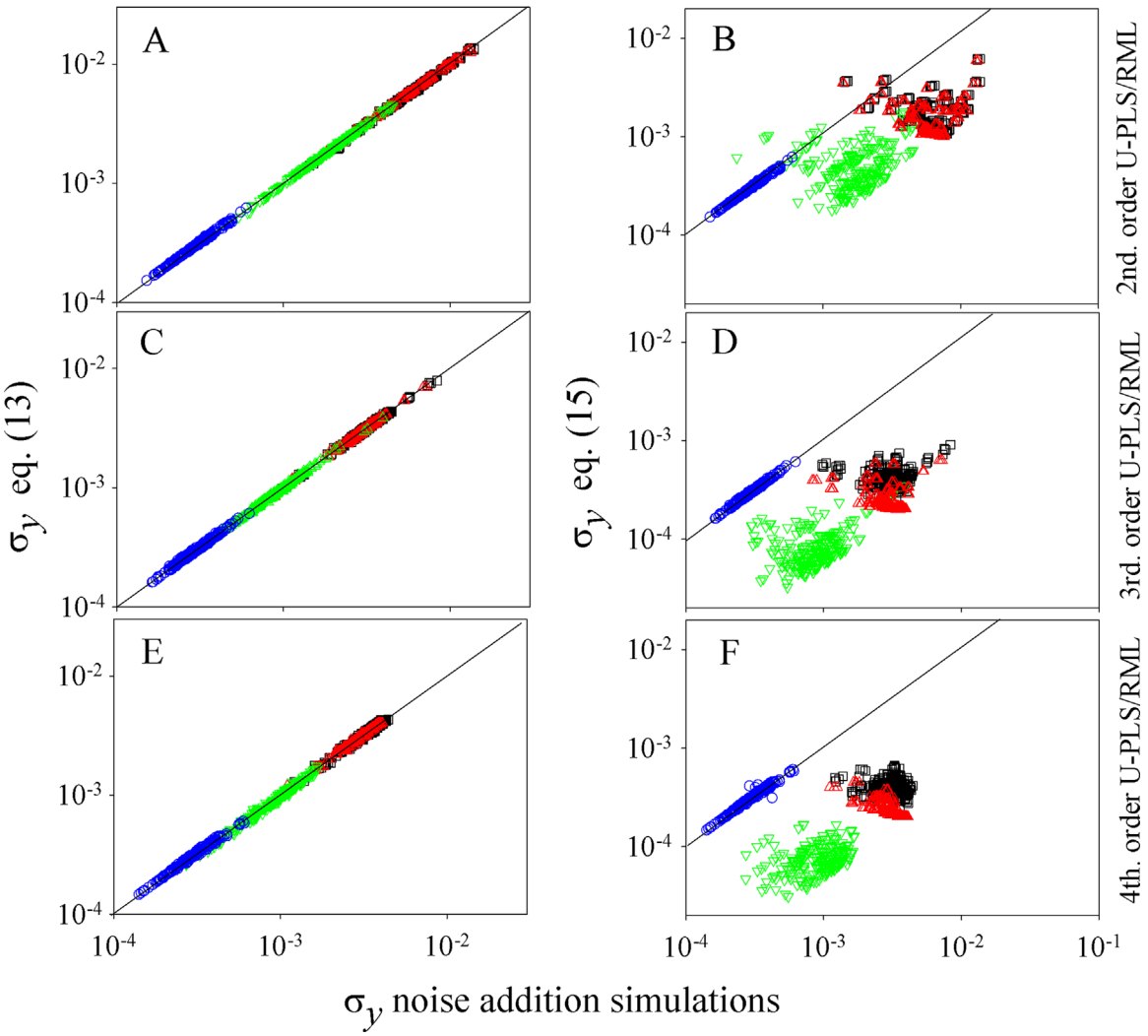

Fig. 3. Plots of calculated uncertainties in predicted concentrations, as a function of noise addition results. The different panels show the results of pink noise addition results over simulated systems in: second-order U-PLS/RML (A and B), third-order U-PLS/RML (C and D), fourth-order U-PLS/RML (E and F). In all plots, the symbols identify the following cases: blue circles, noise only in calibration concentrations, green down triangles, noise only in calibration signals, red up triangles, noise only in test sample signals, and black squares, noise in all concentrations and signals. The thin solid line indicates a perfect correlation. All axes are in logarithmic scale. (For interpretation of the references to color in this figure legend, the reader is referred to the web version of this article.)

However, when an iid structure is assumed, and the variance is estimated from residuals as a unique number, a significant deviation is observed, showing that Eq. (18) is not optimal when trying to estimate uncertainty in the presence of non iid error structures.

4.3. Experimental data

Since in a real experimental data set it is impossible to repeat many calibrations to obtain a reference value of uncertainty, other statistical resources should be applied to compare and contrast the values predicted by the proposed expressions [10]. An alternative is the root mean square error of prediction calculated for a set of test samples ($RMSEP_{test}$). Another possibility is to calculate the standard deviation of a t value (σ_t) [12]. As the estimation of the prediction error improves, this value should approach 1, and the mean standard deviation calculated over all the test samples (MSD_{test}) should resemble the $RMSEP_{test}$ value.

From the bar plot in Fig. 5A, it is evident that $RMSEP_{test}$ is closer to the MSD_{test} estimated under the assumption of a proportional error structure. The same trend is observed when the comparison is made through the σ_t value, which gets closer to 1 when a proportional noise structure is considered along the spectral mode (Fig. 5B). These results confirm once again the importance of having an approximate idea of the error sources that are affecting the system under study, to get to a reliable estimate of the prediction uncertainty.

5. Conclusions

The presently discussed trends clearly show the importance of drawing attention to the different contributions affecting the error structure of the data under analysis to estimate reliable uncertainty values. It is important to note that the proposed approach allows one to estimate prediction uncertainties for different error sources, without depending on the RMSEP value, which is not sample specific. The estimator is also useful to analyze the influence of specific error sources. Further work is required to develop of general strategies to elucidate error sources when the number of replicates is low or when there are no replicates, as well as the to extend the non-iid paradigm to other multi-way algorithms beyond U-PLS/RML.

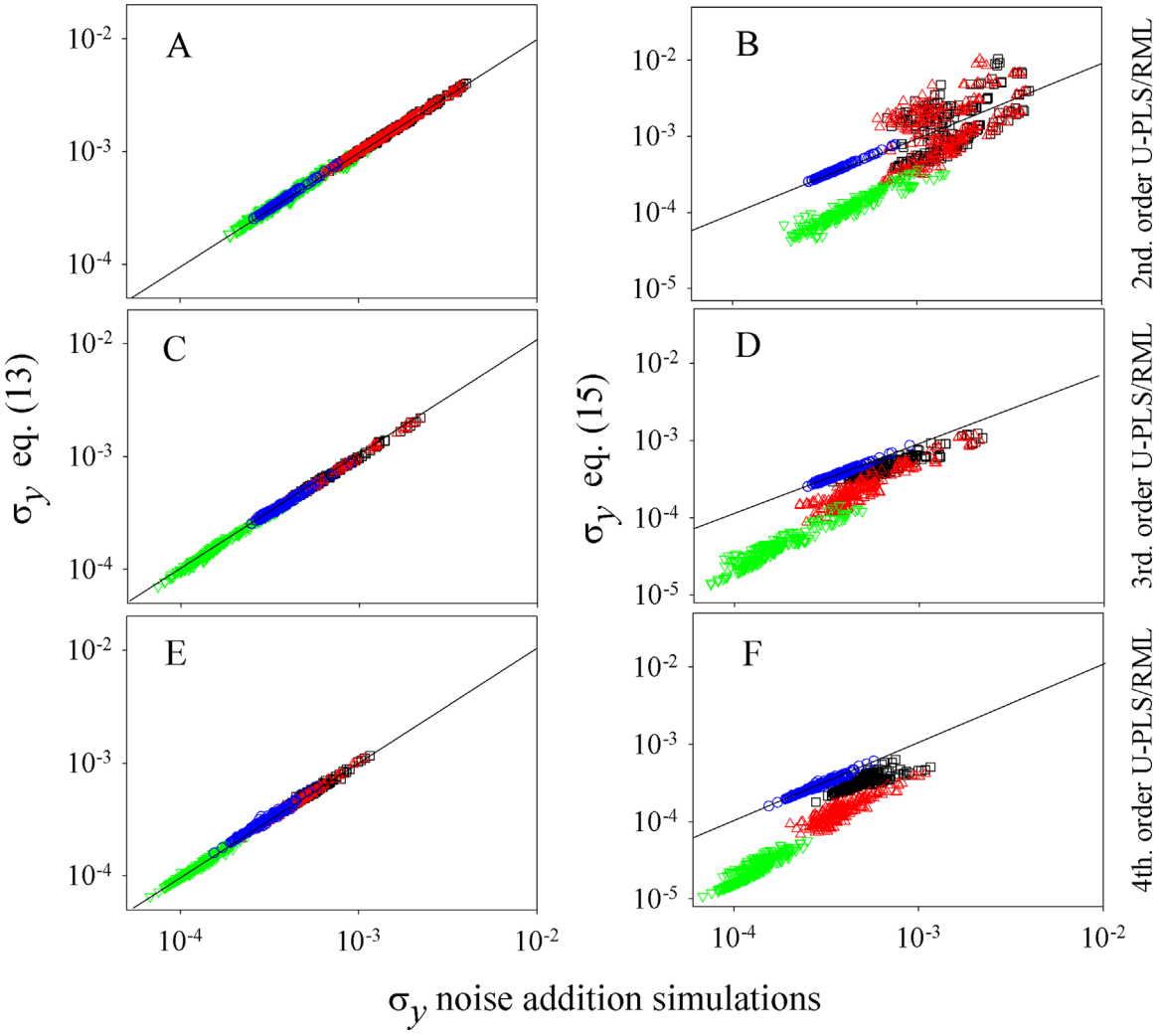

Fig. 4. Plots of calculated uncertainties in predicted concentrations, as a function of noise addition results. The different panels show the results of proportional noise addition results over simulated systems in: second-order U-PLS/RML (A and B), third-order U-PLS/RML (C and D), fourth-order U-PLS/RML (E and F). In all plots, the symbols identify the following cases: blue circles, noise only in calibration concentrations, green down triangles, noise only in calibration signals, red up triangles, noise only in test sample signals, and black squares, noise in all concentrations and signals. The thin solid line indicates perfect correlation. All axes are in logarithmic scale. (For interpretation of the references to color in this figure legend, the reader is referred to the web version of this article.)

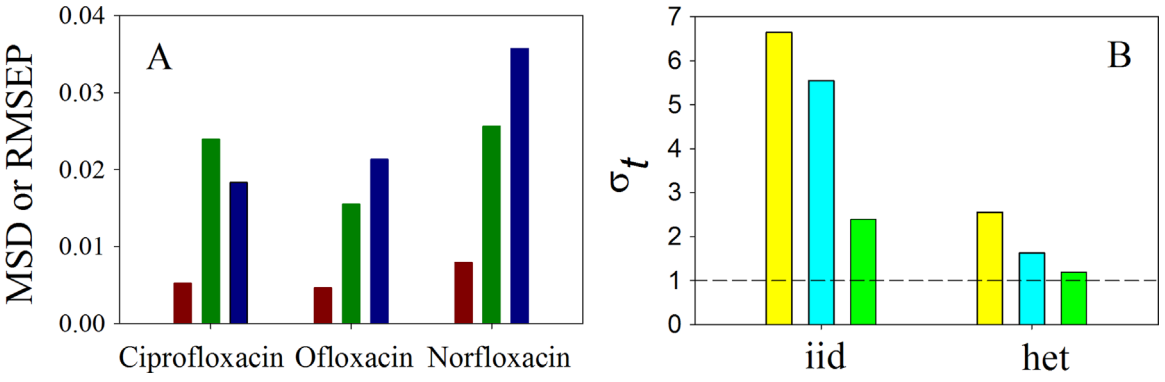

Fig. 5. Bar plots summarizing the results obtained for the experimental data set. (A) Comparison between MSD and RMSEP. Red bars: MSD calculated assuming iid noise structure, green bars: MSD calculated assuming proportional noise in the spectral mode, blue bars: $RMSEP_{test}$. (B) Standard deviation of a t value calculated as $t = \frac{\hat{y} - y_{ref}}{s_{\hat{y}}}$. Yellow bars: σ_t calculated for ciprofloxacin determination in test samples, cyan bars: σ_t calculated for ofloxacin determination in test samples, green bars: σ_t calculated for norfloxacin determination in test samples. (For interpretation of the references to color in this figure legend, the reader is referred to the web version of this article.)

Acknowledgments

Universidad Nacional de Rosario (Project no. 19B/487), CONICET (Consejo Nacional de Investigaciones Científicas y Técnicas, Project no. PIP 0163) and ANPCyT (Agencia Nacional de Promoción Científica y Tecnológica, Project no. PICT-2013-0136) are gratefully acknowledged for financial support. F.A. thanks CONICET for a doctoral fellowship and Fundación Josefina Prats for financial support.

Appendix A.

If **C** is a generic $m \times n$ matrix and **B** is a $p \times q$ matrix, then the Kronecker product **C**⊗**B** is the $mp \times nq$ matrix:

$$\mathrm{C}\otimes\mathrm{B}=\begin{bmatrix} c_{11}\mathrm{B} & \dots & c_{1n}\mathrm{B} \\ \vdots & \ddots & \vdots \\ c_{m1}\mathrm{B} & \dots & c_{mn}\mathrm{B} \end{bmatrix} \tag{A1}$$

If only the first column of **C** (**c**) and **B** (**b**) are taken, the resulting Kronecker product between these vectors can be expressed as:

$$\mathrm{c}\otimes\mathrm{b}=\begin{bmatrix} c_{11}\mathrm{b} \\ \vdots \\ c_{m1}\mathrm{b} \end{bmatrix}=\begin{bmatrix} c_{11}b_{11} \\ c_{11}b_{21} \\ c_{11}b_{p1} \\ \vdots \\ c_{m1}b_{11} \\ c_{m1}b_{21} \\ c_{m1}b_{p1} \end{bmatrix} \tag{A2}$$

For the derivation of Eq. (4), we consider the signal for two interferents modeled by RML ($\mathbf{c}_{\mathrm{int},1}\otimes\mathbf{b}_{\mathrm{int},1}+\mathbf{c}_{\mathrm{int},2}\otimes\mathbf{b}_{\mathrm{int},2}$), having 2 sensors in one mode (represented by matrix **B**, with columns $\mathbf{b}_{\mathrm{int},1}$ and $\mathbf{b}_{\mathrm{int},2}$) and 3 sensors in the other one (represented by matrix **C**, with columns $\mathbf{c}_{\mathrm{int},1}$ and $\mathbf{c}_{\mathrm{int},2}$):

$$\mathbf{c}_{int,1}\otimes\mathbf{b}_{int,1}+\mathbf{c}_{int,2}\otimes\mathbf{b}_{int,2}=\begin{bmatrix} c_{12}b_{12}+c_{12}b_{12} \\ c_{12}b_{22}+c_{12}b_{22} \\ c_{22}b_{12}+c_{22}b_{12} \\ c_{22}b_{22}+c_{22}b_{22} \\ c_{32}b_{12}+c_{32}b_{12} \\ c_{32}b_{22}+c_{32}b_{22} \end{bmatrix} \tag{A3}$$

where the first subscript represents the sensor and the second one the interferent index. The subscript 'int' has been dropped in the right-hand side for simplicity. Differentiation leads to:

$$d(\mathbf{c}_{\mathrm{int},1}\otimes\mathbf{b}_{\mathrm{int},1}+\mathbf{c}_{\mathrm{int},2}\otimes\mathbf{b}_{\mathrm{int},2}) = \begin{bmatrix} c_{11}db_{11}+dc_{11}b_{11}+c_{12}db_{12}+dc_{12}b_{12} \\ c_{11}db_{21}+dc_{11}b_{11}+c_{12}db_{22}+dc_{12}b_{22} \\ c_{211}db_{11}+dc_{21}b_{11}+c_{22}db_{12}+dc_{22}b_{12} \\ c_{21}db_{21}+dc_{21}b_{11}+c_{22}db_{22}+dc_{22}b_{22} \\ c_{31}db_{11}+dc_{31}b_{11}+c_{32}db_{12}+dc_{32}b_{12} \\ c_{31}db_{21}+dc_{31}b_{11}+c_{32}db_{22}+dc_{32}b_{22} \end{bmatrix} \tag{A4}$$

The latter equation can be written as the product of a matrix and a vector of differentials:

$$d(\mathbf{c}_{\mathrm{int},1}\otimes\mathbf{b}_{\mathrm{int},1}+\mathbf{c}_{\mathrm{int},2}\otimes\mathbf{b}_{\mathrm{int},2})=$$

$$=\begin{bmatrix} c_{11} & 0 & b_{11} & 0 & 0 & c_{12} & 0 & b_{12} & 0 & 0 \\ 0 & c_{11} & b_{21} & 0 & 0 & 0 & c_{12} & b_{22} & 0 & 0 \\ c_{21} & 0 & 0 & b_{11} & 0 & c_{22} & 0 & 0 & b_{12} & 0 \\ 0 & c_{21} & 0 & b_{21} & 0 & 0 & c_{22} & 0 & b_{22} & 0 \\ c_{31} & 0 & 0 & 0 & b_{11} & c_{32} & 0 & 0 & 0 & b_{12} \\ 0 & c_{31} & 0 & 0 & b_{21} & 0 & c_{32} & 0 & 0 & b_{22} \end{bmatrix}\begin{bmatrix} db_{11} \\ db_{12} \\ dc_{11} \\ dc_{21} \\ dc_{31} \\ db_{12} \\ db_{22} \\ dc_{12} \\ dc_{22} \\ dc_{32} \end{bmatrix}=$$

$$=\mathbf{Z}_{\mathrm{int}}\left[d\mathbf{b}_{\mathrm{int},1};\ d\mathbf{c}_{\mathrm{int},1};\ d\mathbf{b}_{\mathrm{int},2};\ d\mathbf{c}_{\mathrm{int},2}\right]=$$

$$=\left[\mathbf{c}_{\mathrm{int},1}\otimes\mathbf{I}_2,\ \mathbf{I}_3\otimes\mathbf{b}_{\mathrm{int},1},\ \mathbf{c}_{\mathrm{int},2}\otimes\mathbf{I}_2,\ \mathbf{I}_3\otimes\mathbf{b}_{\mathrm{int},2}\right]$$
$$\left[d\mathbf{b}_{\mathrm{int},1};\ d\mathbf{c}_{\mathrm{int},1};\ d\mathbf{b}_{\mathrm{int},2};\ d\mathbf{c}_{\mathrm{int},2}\right] \tag{A5}$$

where $\mathbf{I}_2$ and $\mathbf{I}_3$ are 2×2 and 3×3 unit matrices respectively.

General $\mathbf{Z}_{\mathrm{int}}$ matrices obtained from RML data processing are provided in Table A.1.

Table A.1
Matrices representing the space spanned by the interferents in multi-way calibration.

Data order	$\mathbf{Z}_{\mathrm{int}}$[a]
2	$[\mathbf{c}_1\otimes\mathbf{I}_J,\ \mathbf{I}_K\otimes\mathbf{b}_1,\ \mathbf{c}_2\otimes\mathbf{I}_J,\ \mathbf{I}_K\otimes\mathbf{b}_2,\ \dots]$
3	$[\mathbf{d}_1\otimes\mathbf{c}_1\otimes\mathbf{I}_J,\ \mathbf{d}_1\otimes\mathbf{I}_K\otimes\mathbf{b}_1,\ \mathbf{I}_L\otimes\mathbf{c}_1\otimes\mathbf{b}_1,\ \mathbf{d}_2\otimes\mathbf{c}_2\otimes\mathbf{I}_J,\ \mathbf{d}_2\otimes\mathbf{I}_K\otimes\mathbf{b}_2,\ \mathbf{I}_L\otimes\mathbf{c}_2\otimes\mathbf{b}_2,\ \dots]$
4	$[\mathbf{e}_1\otimes\mathbf{d}_1\otimes\mathbf{c}_1\otimes\mathbf{I}_J,\ \mathbf{e}_1\otimes\mathbf{d}_1\otimes\mathbf{I}_K\otimes\mathbf{b}_1,\ \mathbf{e}_1\otimes\mathbf{I}_L\otimes\mathbf{c}_1\otimes\mathbf{b}_1,\ \mathbf{I}_M\otimes\mathbf{d}_1\otimes\mathbf{c}_1\otimes\mathbf{b}_1,\ \mathbf{e}_2\otimes\mathbf{d}_2\otimes\mathbf{c}_2\otimes\mathbf{I}_J,\ \mathbf{e}_2\otimes\mathbf{d}_2\otimes\mathbf{I}_K\otimes\mathbf{b}_2,\ \mathbf{e}_2\otimes\mathbf{I}_L\otimes\mathbf{c}_2\otimes\mathbf{b}_2,\ \mathbf{I}_M\otimes\mathbf{d}_2\otimes\mathbf{c}_2\otimes\mathbf{b}_2,\dots]$

[a] The profiles b_1, b_2, c_1, c_2, d_1, d_2, e_1, e_2, … correspond to the interferents in the different data modes. I_J, I_K, I_L and I_M are appropriately dimensioned unit matrices, of size $J \times J$, $K \times K$, $L \times L$ and $M \times M$ respectively. The numbers 1, 2, … run up to the total number of interferents. The subscript 'int' has been dropped for simplicity.

Appendix B. Supporting information

Supplementary data associated with this article can be found in the online version at http://dx.doi.org/10.1016/j.chemolab.2016.09.001.

References

[1] G.M. Escandar, A.C. Olivieri, Practical Three-Way Calibration, Elsevier, Waltham, USA, 2014.
[2] A. Muñoz de la Peña, H.C. Goicoechea, G.M. Escandar, A.C. Olivieri, Fundamentals and Analytical Applications of Multiway Calibration, Data Handling in Science and Technology, Elsevier, Amsterdam, 2015.
[3] A. Smilde, R. Bro, P. Geladi, Multiway Analysis with Applications in the Chemical Sciences, John Wiley & Sons, West Sussex, England, 2004.
[4] A.C. Olivieri, Analytical figures of merit: from univariate to multiway calibration, Chem. Rev. 114 (2014) 5358–5378.
[5] A.C. Olivieri, S. Bortolato, F. Allegrini, Figures of Merit in Multiway Calibration, in Ref. 2, (Chapter 13).
[6] A.C. Olivieri, K. Faber, New developments for the sensitivity estimation in four-way calibration with the quadri-linear parallel factor model, Anal. Chem. 84 (2012) 186–193.
[7] M.C. Bauza, G.A. Ibanez, R. Tauler, A.C. Olivieri, A sensitivity equation for quantitative analysis with multivariate curve resolution – alternating least-squares. Theoretical and experimental approach, Anal. Chem. 84 (2012) 8697–8706.
[8] F. Allegrini, A.C. Olivieri, Analytical figures of merit for partial least-squares coupled to residual multi-linearization, Anal. Chem. 84 (2012) 10823–10830.
[9] P.D. Wentzell, Measurement errors in multivariate chemical data, J. Braz. Chem. Soc. 25 (2014) 183–196.
[10] F. Allegrini, P.D. Wentzell, A.C. Olivieri, Generalized error-dependent prediction uncertainty in multivariate calibration, Anal. Chim. Acta 903 (2016) 51–60.

[11] K. Faber, B.R. Kowalski, Propagation of measurement errors for the validation of predictions obtained by principal component regression and partial least squares, J. Chemom. 11 (1997) 181–238.
[12] N.M. Faber, R. Bro, Standard error of prediction for multiway PLS: 1. Background and a simulation study, Chemom. Intell. Lab. Syst. 61 (2002) 133–149.
[13] K. Danzer, L.A. Currie, Guidelines for calibration in analytical chemistry. Part I. Fundamentals and single component calibration, Pure Appl. Chem. 70 (1998) 993–1014.
[14] K. Danzer, M. Otto, L.A. Currie, Guidelines for calibration in analytical chemistry. Part 2: Multicomponent calibration, Pure Appl. Chem. 76 (2004) 1215–1225.
[15] A.C. Olivieri, N.M. Faber, J. Ferre, R. Boque, J.H. Kalivas, H. Mark, Uncertainty estimation and figures of merit for multivariate calibration, Pure Appl. Chem 78 (2006) 633–661.
[16] P. De Bièvre, Measurement results without statements of reliability (uncertainty) should not be taken seriously, Accredit. Qual. Assur. 2 (1997) 269.
[17] K. Faber, A. Lorber, B.R. Kowalski, Analytical figures of merit for tensorial calibration, J. Chemom. 11 (1997) 419–461.
[18] A.C. Olivieri, G.M. Escandar, H.C. Goicoechea, A. Muñoz de la Peña, Unfolded and Multiway Partial Least-squares with Residual multilinearization: Fundamentals, in Ref. 2, (Chapter 7).
[19] R. Bro, PARAFAC. Tutorial and applications, Chemom. Intell. Lab. Syst. 38 (1997) 149–171.
[20] R. Tauler, Multivariate curve resolution applied to second-order data, Chemom. Intell. Lab. Syst. 30 (1995) 133–146.
[21] MATLAB Version R2012a, The Mathworks, Natick, USA, 2012.
[22] A.C. Olivieri, On a versatile second-order multivariate calibration method based on partial least-squares and residual bilinearization. Second-order advantage and precision properties, J. Chemom. 19 (2005) 253–265.
[23] S.K. Schreyer, M. Bidinosti, P.D. Wentzell, Application of maximum likelihood principal components regression to fluorescence spectra, Appl. Spectrosc. 56 (2002) 789–796.
[24] C.D. Brown, L. Vega-Montoto, P.D. Wentzell, Derivative preprocessing and optimal corrections for baseline drift in multivariate calibration, Appl. Spectrosc. 54 (2000) 1055–1068.
[25] P.D. Wentzell, M.T. Lohnes, Maximum likelihood principal component analysis with correlated measurement errors: theoretical and practical considerations, Chemom. Intell. Lab. Syst. 45 (1999) 65–85.
[26] W.D. Fragoso, F. Allegrini, A.C. Olivieri, A new and consistent parameter for measuring the quality of multivariate analytical methods: generalized analytical sensitivity, Anal. Chim. Acta (2016) (in press).
[27] F. Allegrini, A.C. Olivieri, IUPAC-consistent approach to the limit of detection in partial least-squares calibration, Anal. Chem. 86 (2014) 7858–7866.
[28] M.D. Borraccetti, P.C. Damiani, A.C. Olivieri, When unfolding is better: unique success of unfolded partial least-squares regression with residual bilinearization for the processing of spectral-pH data with strong spectral overlapping. Analysis of fluoroquinolones in human urine based on flow-injection pH-modulated synchronous fluorescence data matrices, Analyst 8 (2009) 1682–1691.
[29] M.N. Leger, L. Vega-Montoto, P.D. Wentzell, Methods for systematic investigation of measurement error covariance matrices, Chemom. Intell. Lab. Syst. 77 (2005) 181–205.